

J. Physiol. (Paris) 00 (2000) 00–00

© 2000 Elsevier Science Ltd. Published by Éditions scientifiques et médicales Elsevier SAS. All rights reserved

PII: S0928-4257(00)01090-1/FLA

## Mesoscopic neurodynamics: From neuron to brain

Walter J. Freeman\*

*Department of Molecular and Cell Biology, University of California, Berkeley, CA 94720-3200, USA*

Received 21 June 2000; accepted 7 August 2000

**Abstract** – Intelligent behavior is characterized by flexible and creative pursuit of endogenously defined goals. Intentionality is a key concept by which to link neuron and brain to goal-directed behavior through brain dynamics. An archetypal form of intentional behavior is an act of observation in space-time, by which information is sought for the guidance of future action to explore unpredictable and ever-changing environments. These acts are based in the brain dynamics that creates spatiotemporal patterns of neural activity, serving as images of goals, of command sequences by which to act to reach goals, and of expected changes in sensory input resulting from intended actions. Prediction of the sensory consequences of intended action and evaluation of performance is by reafference. An intentional act is completed upon modification of the system by itself through learning. These principles are well known among psychologists and philosophers. What is new is the development of nonlinear mesoscopic brain dynamics, by which the theory of chaos can be used to understand and simulate the constructions of meaningful patterns of neural activity that implement the process of observation. The design of neurobiological experiments, analysis of the resulting data, and synthesis of explanatory models require an understanding of the hierarchical nature of brain organization, here conceived as single neurons and neural networks at the microscopic level; clinically defined cortical and subcortical systems studied by brain imaging (for example, fMRI) at the macroscopic level, and self-organizing neural populations at an intermediate mesoscopic level, at which synaptic interactions create novel activity patterns through nonlinear state transitions. The constructive neurodynamics of sensory cortices, when they are engaged in pattern recognition, is revealed by learning-dependent spatial patterns of amplitude modulation and by newly discovered radially symmetric spatial gradients of the phase of aperiodic carrier waves in multichannel subdural EEG recordings. © 2000 Elsevier Science Ltd. Published by Éditions scientifiques et médicales Elsevier SAS

EEG / intentionality / mesoscopic brain dynamics / perception / reafference

### 1. Introduction: intentionality provides the context for brain dynamics

The salient characteristic of animal and human behavior is its directedness toward goals that become apparent as sequences of actions bring the observed person or animal toward a situation or condition that can be identified as capture of something of value, such as food, drink, a mate, or shelter from danger or discomfort. In a broad view these goals are set by and consistent with basic biological requirements for survival and reproduction, but what is more interesting is the manner in which the specific behaviors displayed by organisms that satisfy these requirements emerge from within. The acts are not initiated by events in their environments; they are designed, implemented, and adapted to rapidly changing conditions in the environments by emergent dynamics in the organisms, in the vertebrates primarily through the self-organizing neurodynamics of their forebrains.

These goal-directed behaviors have been known to philosophers as ‘intentional’ since the work of Thomas Aquinas [1], who introduced the term to describe the process by which humans and animals learn about the world by adapting and assimilating to the specific conditions of their environments. A principal problem was how the stimuli coming from the environment could lead to the acquisition of knowledge. He concluded that single events in the material world are not knowable, and that knowledge comes only through abstraction and generalization from the ‘phantasmata’ of raw sensory impacts.

This conclusion is immediately relevant to experimental findings that are reviewed here. In particular, when the neural activity evoked by a stimulus is observed in the brains of small animals that have been trained to respond behaviorally, it is clear that the microscopic patterns forced by single stimuli are not retained, and that they lead to replacement by a mesoscopic activity pattern [14] constituting a generalization over the class of stimuli [12]. This review is devoted to a description of this process of generalization and related operations of brain dynamics in the context of intentionality.

\* Correspondence and reprints.

*E-mail address:* wfreeman@socrates.berkeley.edu (W.J. Freeman).

### *1.1. A brief overview of intentionality governing an act of observation*

The first step in pursuit of an understanding of the neurodynamics of intentionality is to ask, what happens in brains during an act of observation? This is not a passive receipt of information from the world. It is a purposive action by which an observer directs the sense organs toward a selected aspect of the world and selects from the resulting barrage of sensory stimuli the small fraction that is relevant to the intent of the action. The concept of intentionality was used by Aquinas to describe this action-perception cycle in both animals and humans, while distinguishing it from volition, which involved awareness of the ethical dimensions of action. Three salient characteristics of intentionality that can be inferred from his work are (a) intent, (b) wholeness, and (c) unity [12].

(a) Intent (from the Latin word ‘intendere’, meaning thrusting forth) comprises the endogenous initiation, construction, and direction of behaviors into the world, followed by learning from the consequences of the behaviors. It is the process that governs Merleau-Ponty’s [39] ‘intentional arc’. It emerges within brains. Agents including humans, animals and perhaps autonomous robots select their own goals, plan their own tactics, and choose when to begin, modify, and stop sequences of action. They learn about their environments by assimilation (from the Latin word ‘adequatio’, meaning approaching equivalence, like the way a hand is shaped to the form of a cup for drinking). Humans at least are subjectively aware of themselves acting, but consciousness is not a necessary property of intention; in any case, studies of scalp event-related potentials by Walter [58], Kornhuber and Deecke [36], and Libet [37] indicate that humans become aware of their intentions only in the course of unfolding their intended behaviors after they have been initiated, so that intentional action precedes consciousness.

(b) Unity is inherent in the combining of input from all sensory modalities into gestalts, and in the coordination of all parts of the body, both musculoskeletal and autonomic, into adaptive, flexible, yet integrated movements through the motor neurons in what Sherrington in 1906 [41] called ‘the final common path’. Subjectively, unity appears in the awareness of self and its feelings of emotion, but again this is not prerequisite for unity, in that intentional actions are commonly not conscious.

(c) Wholeness is revealed by the orderly changes in the self and its behavior that constitute the

development, maturation and adaptation of the self, within the constraints of its genes or design principles, and its material, social and industrial environments. Subjectively, wholeness is revealed in the remembrance of self through a lifetime of change. The influences of accumulated and integrated experience on current behavior are not dependent on explicit recollection and recognition. In brief, the study of intentionality can be directed toward understanding the neural mechanisms by which goal states and goal-directed behaviors are constructed, executed, and evaluated, while avoiding invoking the subjective processes of consciousness, awareness and emotion. The prototype of intentional behavior can be found in a directed, purposive act of looking, listening, touching, or sniffing, irrespective of whether the observer, animal or human, is or is not conscious of the act and its results.

These aspects of intentionality correspond roughly to three current uses of the term. In psychology it means purpose, as in ‘He intended to do an experiment’. Intent is often conflated by psychologists with motivation, but not so by lawyers, who distinguish between intent as that which is to be done, and motive as the reason for the intent. In medicine and surgery, it means the modes of healing and re-integration of the body after damage; healing by first intention leaves a clean scar; healing by second intention is accompanied by the flow of pus. These uses began early in the 14th century, when the philosophy of Aquinas was gaining wide acceptance, and have persisted. Among medieval philosophers knowledge by first intention was immediate sense experience, and knowledge by reflection was by second intention. In the 20th century analytic philosophers use ‘intentionality’ to mean the way in which beliefs, thoughts and images (mental ‘representations’) are connected with (‘about’) objects and events in the world. This is also known as the symbol-grounding problem: how are representations in brains and computers to be attached to the things they represent? The Aquinian view avoids and disavows ‘representations’ as Platonic forms, and instead posits forms that are created intentionally by the ‘imagination’. These forms and the mesoscopic dynamics by which they are created are the objects of our search in animal brains.

### *1.2. Sensorimotor and limbic cortices are organs of intentional behavior*

Brain scientists have known for over a century that the necessary and sufficient part of the verte-

brate brain to sustain minimal intentional behavior is the medioventral forebrain, including those components that comprise the external shell of the phylogenetically oldest part of the forebrain, the archicortex and paleocortex, the deeper lying nuclei with which the cortices are connected, and the olfactory bulb that receives direct sensory input from olfactory receptors. These components suffice to support remarkably adept patterns of intentional behavior in dogs after all the newer parts of the forebrain were surgically removed by Goltz [23], and in rats with neocortex chemically inactivated by spreading depression as shown by Bures et al. [3]. In contrast, intentional behavior is severely altered or absent after major damage to the medial temporal lobe of the basal forebrain bilaterally, as manifested for example in Alzheimer's disease.

Phylogenetic evidence comes from observing intentional behavior in salamanders, which have the simplest of the existing vertebrate forebrains [29, 40]. The three main parts are sensory (which, as in small mammals, is predominantly olfactory), motor, and associational (*figure 1*).

These parts can be judged to comprise the limbic system in all vertebrates, but salamander have virtually none of the 'add-ons' found in brains of higher vertebrates, hence the simplicity. The associational part contains the primordial hippocampus, which is identified in higher vertebrates as the locus of the functions of spatial orientation (the 'cognitive map' of Tolman [51] and O'Keefe and Nadel [40]) and temporal integration in learning

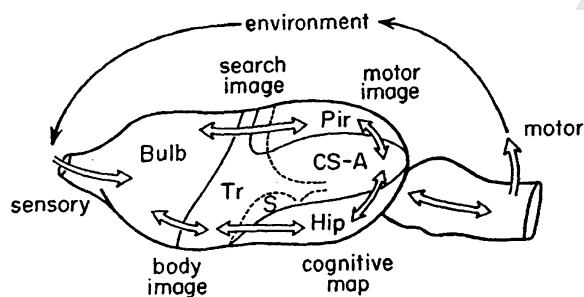


**Fig. 1.** This schematic illustrates the sensory, motor, and associational components of the right hemisphere (seen from above) of the simplest extant vertebrate brain, found in the salamander. The bidirectional connections between these forebrain subdivisions provide for the macroscopic interactions that support the neurodynamics of intentionality: goal formation, action, perception, and learning from the sensory consequences of the actions. These components are the prototype of the limbic system, which in mammals are typically buried by exuberant growth of other 'add-on' structures that operate in and in concert with the limbic system.

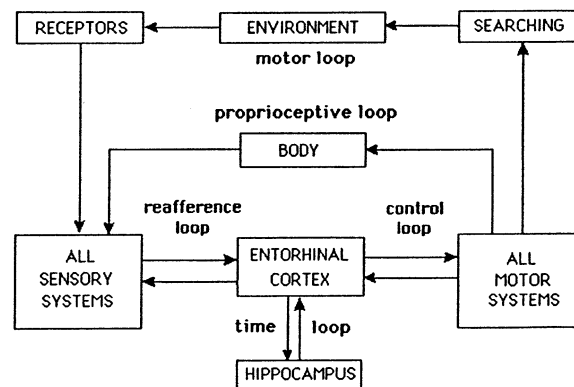


**Fig. 2.** This diagram of brain state space maps the multiple feedback loops that support the intentional arc. In mammals the entorhinal cortex is a key structure. Its most immediate interaction is with the hippocampus, involving temporal integration. Interactions are sustained through longer loops with all of the primary receiving areas, supporting refference [57], and with motor systems in the brainstem, cerebellum and neocortex, subserving motor control. Longer loops pass through the body in proprioception, and through the environment in intentional action.

(the organization of long term and short term memory), operating through the septal nuclei and hypothalamus to control the autonomic and endocrine systems, and through the amygdaloid and striatal nuclei to control the musculoskeletal apparatus. These processes are essential for intentionality, because intentional action takes place into the world, and even to execute the simplest action, such as searching for food or evading a predator, an animal must make decisions and plan actions based on where it is with respect to its world, where its prey or refuge is or is predicted to be, and what its spatial and temporal progress is during sequences of attack or escape. It must mobilize its cardiovascular, respiratory, and metabolic systems to meet the demands on its muscles, and it must have feedback to assay its progress and resources at each step of the action. Multiple feedback loops interconnect numerous structures with each other inside the brain, out through the body, and out through the environment (*figure 2*). These connections support the flow of neural and behavioral activity that is required for the neurodynamics of intentionality.

## 2. Observation of mesoscopic states by recording multichannel EEGs

The crucial question for neuroscientists is, how are the patterns of neural activity that sustain

intentional behavior constructed in brains prior to perception? An answer is provided by studies of electrical activity, the electroencephalogram (EEG) recorded from the pial surfaces of primary sensory areas in animals trained to respond to conditioned stimuli [2, 9, 13, 14, 20, 53].

### 2.1. Mesoscopic neurodynamics of the olfactory system

The most detailed studies have been devoted to the olfactory system [14]. The main findings are as follows. Arrays of closely spaced electrodes ( $8 \times 8$  with 0.5 mm spacing giving a window of  $4 \times 4$  mm) placed on the olfactory bulb, nucleus, or prepyriform cortex show continual background EEG activity having two main components. In the gamma range (20–80 Hz in rabbits) there are bursts of oscillations at continually varying frequencies, which gives spectra of the EEG the form of  $1/f^\alpha$  (where  $\alpha = 2 \pm 1$  and log power decreases linearly with approximately the square of log frequency). The bursts recur at the rate of respiration, generally in the theta range (2–7 Hz), accompanied by a slow wave in the EEG that has a negative peak following inhalation and usually corresponding to the onset of a burst (figure 3). The same wave form is found on all electrodes within the same structure of recording, but with differing spatial patterns of phase and amplitude.

Unlike the time series of the EEG, which shows no relation to odorants, the spatial pattern of amplitude modulation (AM) changes significantly

under both aversive and appetitive classical conditioning to odorants [21]. Changes in AM pattern are progressive over both serial [19] and concomitant discriminative conditioning [55], so that when a new AM pattern forms with learning, or when the significance of an odorant pair is changed by reversing the contingency of reinforcement, all pre-existing AM patterns change slightly but significantly [19, 20]. The AM patterns lack invariance with respect to conditioned stimuli, as shown most clearly under serial conditioning; when an odorant is re-introduced after conditioning to intervening stimuli, the AM pattern changes to a new form and does not recur to a pre-existing form (figure 4).

An interpretation of these findings is that with each inhalation the olfactory receptors excite the bulb and depolarize the bulbar neurons, giving rise to the slow respiratory wave, in which surface negativity manifests excitation. The bulbar neurons have a nonlinear input-output relation known as the 'sigmoid curve' (figure 5), for which the slope shows their strength of transmission or 'gain'. Excitation increases the gain to a threshold where the synaptic interaction in the bulb increases explosively. This increase is analogous to the change in state of a single axon, which is forced by dendritic current across its threshold. That is, the burst of cortical activity is comparable to the action potential of a neuron. In each case the system undergoes a state transition from a receptive (diastolic) mode to a transmitting (systolic) mode. Most of the synapses received by bulbar

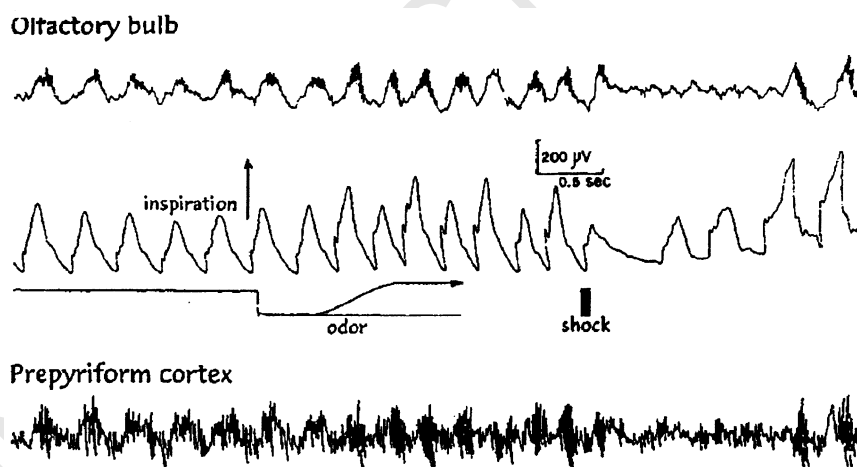
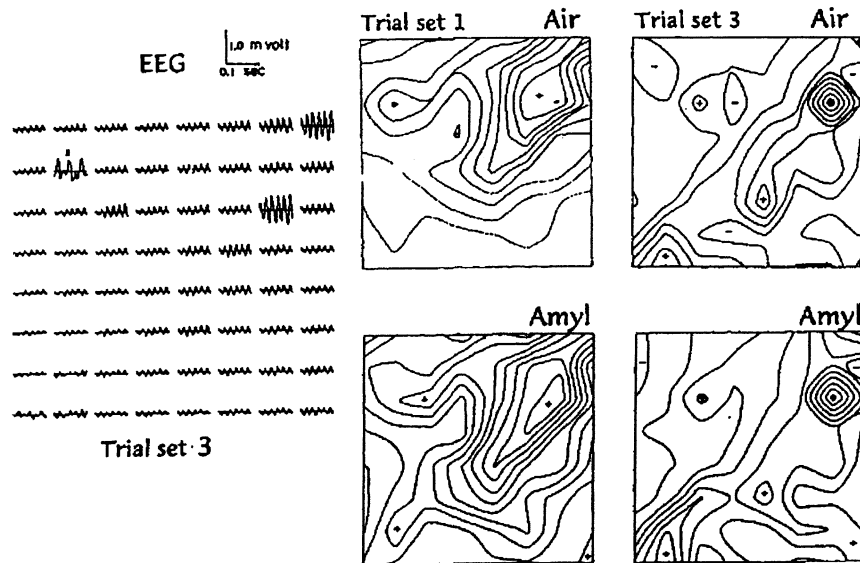


Fig. 3. EEGs are shown from electrodes in the olfactory bulb and prepyriform cortex, and respiration is shown by a pneumograph tracing, during a trial in which an odorant conditioned stimulus is followed by a weak electric shock to the cheek in classical aversive conditioning. The surge of receptor input on inhalation excites the bulb (negative slow wave) and destabilizes it, leading to the gamma bursts.



**Fig. 4.** A representative set of 64 traces is shown from an  $8 \times 8$  array ( $4 \times 4$  mm) placed on the surface of the olfactory bulb (left is anterior), filtered at 20–80 Hz to display the gamma range. The contour plots of amplitude contrast the differences in AM patterns between the control and test periods prior to and during odorant delivery. The changes between trials set 2 weeks apart demonstrate the context dependence and lack of invariance of AM patterns with respect to the control and conditioned stimuli, which were unchanged.

neurons come from other bulbar neurons and not from receptors, which indicates that in the regeneratively excited state the dominant input to each bulbar neuron is by synapses from other bulbar neurons instead of receptor axons. These synapses from internally originating axons are the ones that are modified by learning [7, 8].

These findings lead to the conclusion that the AM patterns are determined not by immediate receptor input but by cumulative synaptic changes with experience. The construction is not by recall of stored patterns but by pattern formation in a distributed nonlinear systems with connections that have been modified through learning. The manner in which this take place involves hierarchical ordering of neural activity between microscopic and mesoscopic levels having differing time and space scales. Central neurons are selectively activated by sensory receptors and driven to generate microscopic activity in the form of trains of action potentials (pulses) on their axons. These and all other neurons in the bulb by their synaptic interactions form a population that 'binds' their activity into a mesoscopic pattern, which expresses the experience with the stimulus and not the presentation of the stimulus.

The significance of this process of AM pattern creation can be seen in terms of the variability of the selection of olfactory receptors that are excited

on each inhalation of the same odorant. Owing to the small sample with each sniff and to the turbulence of air flow in the nose, the receptor pattern must differ with each trial, and it cannot be known, either by the animal or by the experimenter. The action of the bulb is to create by synaptic changes with learning a class to which equivalent receptors can gain access, and it is this class that is manifested by the AM pattern in the EEG. The formation of an AM pattern is by three operations requiring multiple sniffs for learning. One is habituation by which bulbar responses to unwanted input on non-reinforced trials are suppressed. The second is Hebbian learning by which the synapses between pairs of co-excited neurons are strengthened [8, 10, 11]. The third step is read-out from the bulb to the prepyriform cortex. The pathway over which this is done is unlike the input pathway to the bulb, which like all other sensory pathways has a topographic projection. The output pathway is divergent-convergent, meaning that each bulbar neuron transmits broadly, and conversely each receiving cortical neuron receives simultaneously from widely distributed neurons in the bulb. The only bulbar activity that is enhanced by the resulting spatiotemporal integral transformation of the bulbar output is that which has a common instantaneous frequency, and that frequency is the carrier wave

of the AM pattern formed by cooperative interaction. The sensory-driven microscopic activity is not temporally coherent, so it is attenuated. As the result, what the brain receives from the bulb is what the bulb has constructed within itself, not the specific information that has been imposed by receptors during a sniff.

Together these three operations (habituation, association, and spatiotemporal integration) provide the abstraction and generalization that is necessary for the acquisition of knowledge in the sense prescribed by Aquinas. It is noteworthy here that the ‘binding’ of neural activity is not that of ‘feature detector’ neurons in discrete networks performing logical operations by synchronization of firing to ‘represent’ an object [25, 42]. It is the creation of a new AM pattern of activity that embodies cumulative past experience with an odorant upon presentation of that odorant, which enables the animal to modify itself in adding to its experience and to prepare itself for the next appropriate action. As noted also by Hardcastle [27] and long before by Aquinas [1], there is no basis for representation of individual stimuli.

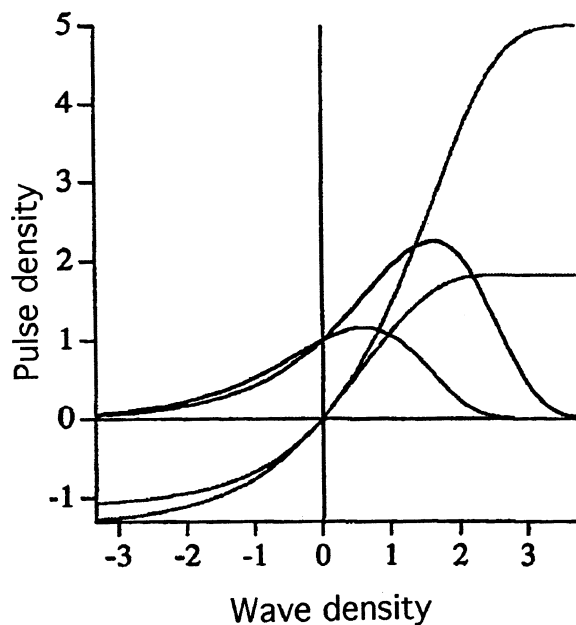


**Fig. 5.** The sigmoid curve is shown for two values of  $Q_m = 1.82$  and  $5.0$ , with normalized pulse density,  $q$ , as a function of normalized wave density,  $v$ , where  $Q_m$  is the upper asymptote of  $q$ . The derivative of the function,  $dq/dv$ , gives the nonlinear gain. The peak gain is at the wave value,  $v_{max}$  (from [18]).

$$q = \exp[-(e^v - 1)/Q_m], \quad dp/dv = \exp[v - (e^v - 1)/Q_m], \quad v_{max} = \ln(Q_m). \quad (1)$$

## 2.2. Evidence from neocortical EEGs concerning reafference

The existence of comparable AM patterns has now been demonstrated in the visual, auditory, and somesthetic cortices [2]. The EEGs from arrays of electrodes on the pial surfaces show a common aperiodic wave form on all electrodes, with a broad ‘ $1/f^2$ ’ spectrum and with spatial AM patterns that change with learning, which can serve as the basis for retrospective classification of trials under discriminative conditioning. The AM patterns are discrete events lasting 80–120 ms and recurring also at rates in the theta range, like frames in a motion picture. The same lack of invariance with respect to conditioned stimuli is found with learning new stimuli in the appropriate modality, and with contingency reversal. Each learned stimulus serves to elicit the construction of a pattern that is shaped by the synaptic modifications between cortical neurons from prior learning, which vastly outnumber the synapses formed by incoming sensory axons, and also by the brain stem nuclei that bathe the forebrain in neuromodulatory chemicals. Each cortical activity pattern is a dynamic operator that creates and carries the meanings of stimuli for the recipient animal. It reflects the individual history, present context, and expectancy, corresponding to the wholeness of the intentionality. The patterns created in each cortex are unique to each animal. All sensory cortices transmit their output in the form of patterns of microscopic action potentials into the limbic system, where they are combined to form gestalts.

Here it is important to review the architecture of perceptual dynamics (*figure 2*). The mesoscopic patterns that in mammals converge to the entorhinal cortex, prior to delivery into the hippocampus for integration over time, all have the same ‘format’. This indicates that the several AM patterns carried by action potentials can be as easily integrated with each other as was the case with the microscopic sensory input to each primary cortex by sensory action potentials, leading to the formation of its mesoscopic pattern. The combined entorhinal signal is sent from the outer three layers mainly by the perforant path to the hippocampus, and it is the main source of hippocampal input. The main target of hippocampal output in mammals is back to the inner three layers of the entorhinal cortex. Then the main target of transmission of the resultant integrated activity patterns is back to the primary sensory cortices. By this architecture whatever signal that is provided by

each sensory port is combined and shared by re-direction back to the incoming ports. This recursive architecture and process has been called 'reafference' [12, 50, 57], 'corollary discharge' [46], and 'preafference' [33]. Evidence for corollary discharges has been found in simultaneous recordings from the bulb, pyriform, entorhinal cortex, and dentate fascia in the hippocampus [34], showing that prior to the arrival of an expected volley from an odorant, the olfactory bulb is prepared by brief, staccato signals from the entorhinal cortex to prime it for that stimulus.

This process was discovered by Helmholtz [28] in studies of patients with injury to the oculomotor nerve, who reported that when they attempted to move their eyes laterally, their visual field appeared to move in the opposite direction. He also observed that a patient who moved his eyeball passively reported that the world appeared to move, which it did not if the subject moved his eye intentionally. He inferred that intentional eye movement was accompanied by a discharge from the motor centers into the visual cortex, which provided the basis for distinguishing movement of objects in the visual field from apparent motion attributable to a movement of eyes or the head. He concluded that "an impulse of the will" that accompanied intentional behavior was unmasked by the paralysis. J. Hughlings Jackson [30] repeated the observations, but postulated alternatively that the phenomenon was caused by 'an in-going current', which was a signal from the non-paralyzed eye that moved too far in the attempt to fixate an object, and which was not a recursive signal from a 'motor centre'. He was joined in this interpretation by William James [31] and Edward Titchener [50], thus delaying deployment of the concepts of neural feedback in re-entrant cognitive processes until late in the 20th century.

### 3. Characteristics of mesoscopic dynamic brain states

The 'state' of the brain is a description of what it is doing in some specified time period. A state transition occurs when the brain changes and does something else. For example, locomotion is a state, within which walking is a rhythmic pattern of activity that involves large parts of the brain, spinal cord, muscles and bones. The entire neuromuscular system changes almost instantly with the transition to a pattern of jogging or running. Similarly, a sleeping state can be taken as a whole,

or divided into a sequence of slow wave and REM stages. Transit to a waking state can occur in a fraction of a second, whereby the entire brain and body shift gears, so to speak. The state of a neuron can be described as active and firing or as silent, with sudden changes in the firing manifesting state transitions. Populations of neurons also have a range of states, which are revealed by their characteristic wave forms, such as in slow wave sleep, fast activity in REM, epileptiform spikes in seizures, or the silence of brain death. The mathematics of nonlinear dynamics is designed to study these states and the transitions by which they are accessed and abandoned [10, 11, 13, 14].

#### 3.1. Evaluation of the stability and destabilization of mesoscopic states

A critical question to ask about the state of a system is its degree of stability or resistance to change. Evaluation is done by perturbing it and observing over what range of intensity of perturbation it returns to its initial state [9, 11]. For example, an object like an egg on a flat surface is unstable, but a coffee mug is stable. A person standing on a moving bus and holding on to a railing is stable, but someone walking in the aisle is not. If a person regains his chosen posture after each perturbation, no matter in which direction the displacement occurred, that state is regarded as stable, and it is said to be governed by an attractor. This is a metaphor to say that the system goes ('is attracted') to the state through an interim state of transience. The range of displacement from which recovery can occur defines the basin of attraction, in analogy to a ball rolling to the bottom of a bowl. If the perturbation is so strong that it causes concussion or a broken leg, and the person cannot stand up again, then the system has been placed outside its prior basin of attraction, and a new state supervenes with its own attractor and basin.

Stability is always relative to the time duration of observation and the criteria for what is chosen to be observed. In the perspective of a lifetime, brains appear to be highly stable, in their numbers of neurons, their architectures and major patterns of connection, and in the patterns of behavior they produce, including the character and identity of the individual that can be recognized and followed for many years. Brains undergo repeated transitions from waking to sleeping and back again, coming up refreshed with a good night or irritable with insomnia, but still, giving arguably the same

persons as the night before. Personal identity is usually quite stable. But in the perspective of the short term, brains are highly unstable. Thoughts go fleeting through awareness, and the face and body twitch with the passing of emotions. Glimpses of their internal states of neural activity reveal patterns that are more like hurricanes than the orderly march of symbols in a computer. Brain states and the states of populations of neurons that interact to give brain function, are highly irregular in spatial form and time course. They emerge, persist for a small fraction of a second, then disappear and are replaced by other states. Yet by the criterion of the statistical parameters of the electrical pulse and EEG activities of its populations of neurons, the waking cerebral cortex is remarkably robust. The stability is readily demonstrated by perturbation with sensory and electrical afferent stimuli, which displace the cortex briefly from its background level of activity, to which it returns by relaxation in a trajectory that is manifested in ‘event-related potentials’. The range of stimulation over which the return can take place defines the basin of attraction for the background attractor. Parameters such as the intensity at which there is failure to return owing to the onset of epileptic seizure, or the duration at which excessive repetition induces sleep, define the boundary or ‘separatrix’ of the waking basin from other basins in a ‘landscape’ of cortical basins of attraction.

### 3.2. Three types of stable cortical states

In using dynamics we define several kinds of stable state, each with its type of attractor. The simplest is the point attractor. The system is at rest in an unchanging steady state unless perturbed, and it returns to rest when it is allowed to do so. As it relaxes to rest as when an area of cortex generates an evoked potential, it has the history of what happened, but that history is lost after convergence to rest. Examples of point attractors are silent neurons or populations that have been isolated from the rest of the brain, and also the brain that is depressed into inactivity by injury or by deep anesthesia, to the point where the EEG has gone flat (*figure 6*, bottom trace; *figure 7*, vertical line at the base; *figure 8*, lowest frame).

A special case of a point attractor is noise. This noise is observed at the microscopic level in populations of neurons in the cortex that are coupled by synaptic excitatory feedback, without need for

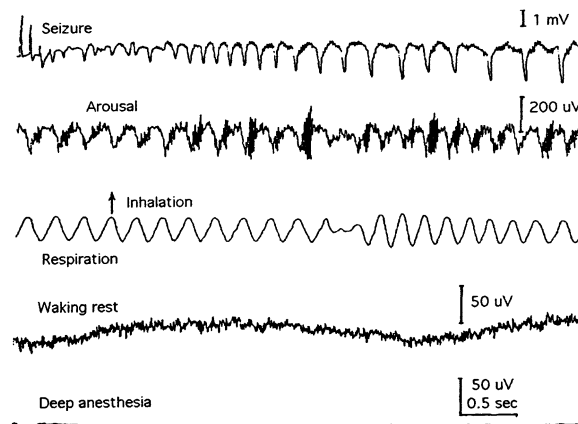


**Fig. 6.** Four levels of function of the olfactory system are revealed by EEG recording. The lowest is the non-interactive ‘open loop’ state [14] imposed by deep anesthesia, which suppresses brain activity. The next is the awake state of rest with aperiodic waves giving a ‘ $1/f^2$ ’ spectrum. The level in which behavior is generated reveals recurrent state transitions with inhalation, by which bursts are formed that reveal spatial patterns of AM (amplitude modulation) relating to odorant recognition. The upper trace shows the pattern of high-amplitude spikes sustained at 3/s when an epileptic seizure has been triggered by intense electrical stimulation. This state is likewise chaotic, but with a reduced correlation dimension (from [45]).

inhibition, because their interactive state is stabilized by the refractory periods of neurons in populations [9, 11, 13]. The neurons fire continually at irregular times, so that their autocorrelation functions go rapidly to zero, and their interval histograms decay exponentially after a dead time imposed by the absolute and relative refractory periods of the action potentials. Their crosscorrelation functions likewise are near zero, because they do not fire in concert with each other. Knowledge about the prior pulse trains from each neuron and those of its neighbors up to the present fails to support prediction of when the next pulse will occur. The state of noise has continual activity with no history of how it started, and it gives only the expectation that its mean and higher order statistical properties will persist as in the recent past. Simulation of the stable and sustained output of a population of mutually excitatory neurons is shown in *figure 9*.

An amplitude histogram of the pulse density of neurons in local neighborhoods at the mesoscopic level shows a Gaussian distribution about a mean value (*figure 10*), which is restricted to the upper region of the nonlinear sigmoid gain curve (*figure 5*) that specifies the relation between the dendritic current density,  $v$ , and the axonal pulse density,  $q$ ,

of neural populations in normalized coordinates [14]. The derivative of the sigmoid curve reveals the nonlinear gain,  $dq/dv$ . In the upper region,  $v > v_{\max}$ , an excitatory perturbation increases the excitatory activity of the population and decreases the gain, owing to the cumulative effects of the refractory periods, and when the gain goes down, the level of evoked activity decreases until the activity has returned to the self-sustained activity level. Any decrease in activity is accompanied by an increase in gain, which is followed by a compensatory homeostatic increase in activity. Thus the stability of the self-sustaining state is revealed by perturbation [14] to have the form of a point attractor. At the microscopic level, the self-sustained activity appears densely packed action potentials ('noise'), and at the mesoscopic level it appears as an excitatory bias (figure 9, top trace). The power spectral density has the  $1/f^2$  form (figure 10, upper frame) that corresponds to the spectrum of 'brown noise' created by 'white noise' passed through a two-pole low-pass filter).

The interaction of excitatory neuron populations with inhibitory populations at the mesoscopic level gives sustained oscillation. In some conditions imposed by surgical or pharmacological isolation of the olfactory bulb [14], the oscillation may take the form of a sinusoidal wave [9, 18] that

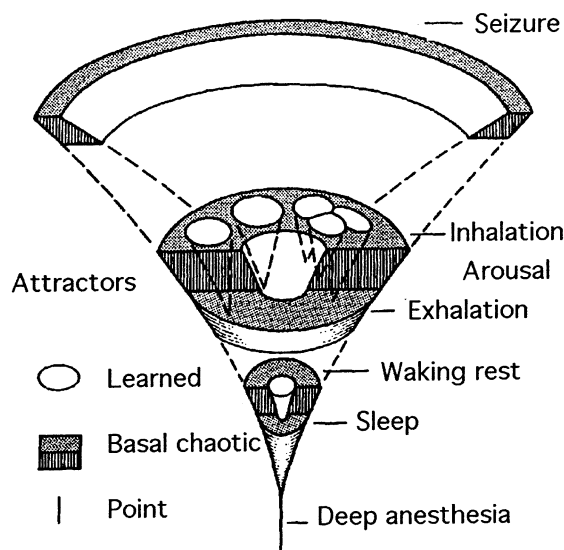


**Fig. 7.** The four states of the olfactory system as revealed by EEGs are linked in a bifurcation diagram, in which the amplitude of olfactory neural activity controlled by brainstem mechanisms serving arousal is used as a bifurcation parameter (from [45]).

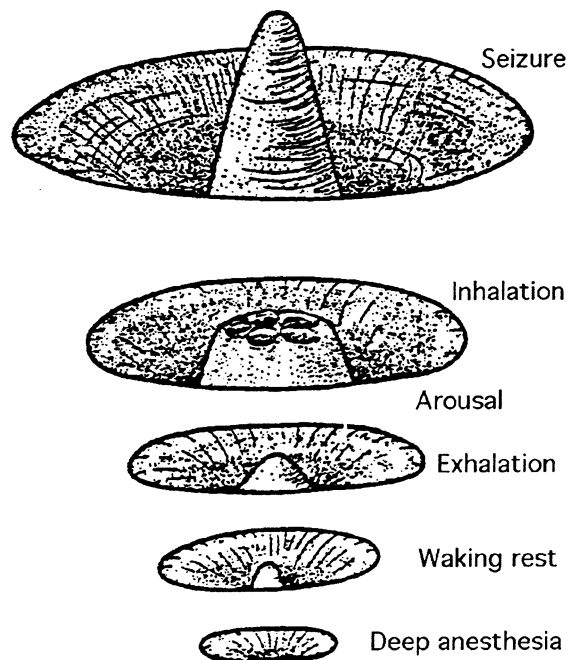


**Fig. 8.** This perspective offers a hypothesis of how an attractor landscape of learned basins of attraction is created with each inhalation. The selection of a basin is made by the input odorant. If the stimulus is novel or unknown, an orienting behavior occurs ('I don't know'), and the system goes into the surrounding chaotic basin, which provides the aperiodic unpatterned activity that drives Hebbian learning for formation of a new basin. Attractor crowding [59] then changes all of the other basins, resulting in contextual pattern dependence (figure 4) (from [45]).

gives a peak at one frequency in the power spectral density. An open system that gives periodic behavior is said to be governed by a limit cycle attractor. The classic example is a wrist watch. If it keeps good time despite being knocked about, it is stable, but if it winds down and runs out of power, it becomes unstable and switches to a point attractor. Its history is then limited to one cycle, after which there is no retention of its transient approach in its basin to its attractor. Neurons and populations do not usually fire periodically, and when they appear to do so, close inspection shows that the activities are in fact somewhat irregular and unpredictable in detail. When nearly periodic activity does occur, at the microscopic level it is due to injury or pacemaker potentials. At the mesoscopic level it is seen in the olfactory bulb when it has been surgically or cryogenically isolated from the rest of the system [14]. At the macroscopic level of behavior, periodicity is either intentional, as in rhythmic drumming, clapping

and dancing, or it is pathological, as in the periodic oscillations of the eyes in nystagmus or of the limbs during Parkinsonian tremor or of the cortex during the hypersynchrony of partial complex seizures that are revealed by near-periodic spike trains (figure 6, top trace). The reason that limit cycle oscillation is uncommon at the mesoscopic level is that the feedback is nonlinear. The wave density and pulse densities show Gaussian distributions (figure 11) about a mean that is located on the low amplitude segment of the sigmoid function, below the peak of the nonlinear gain (figure 5). When activity levels increase, the gain increases, causing a regenerative positive feedback that increases activity still further. This nonlinearity is the basis for the nonlinear state transitions that recur with respiration in the olfactory system (figure 3).

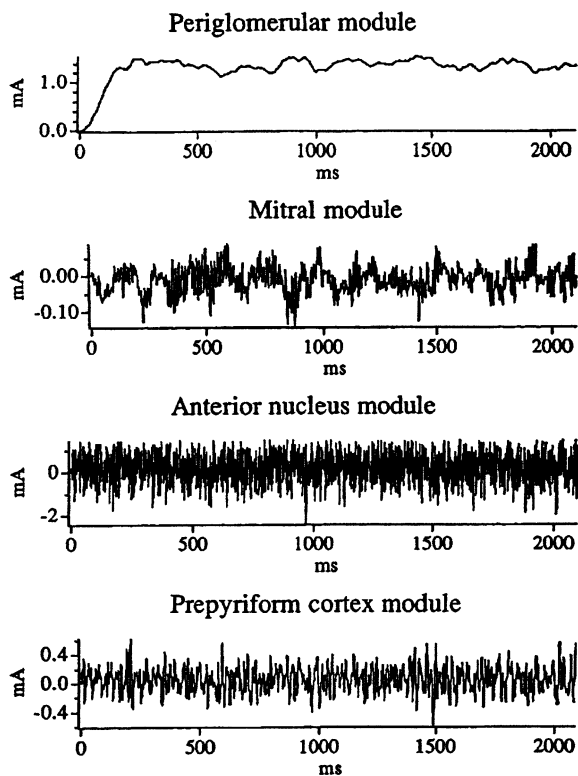


Fig. 9. Representative state variables in a 2 s time period are shown from a set of coupled nonlinear ordinary differential equations solved on a digital computer. Random number generators were used to simulate the noise to stabilize chaotic dynamics. The EEGs and pulse densities observed in the various parts of the olfactory system were simulated. Although the several parts are continuously interacting to generate the aperiodic time series, the crosscorrelations between the traces average near zero, illustrating the failure of techniques of linear correlation to detect nonlinear interactions (from [18]).

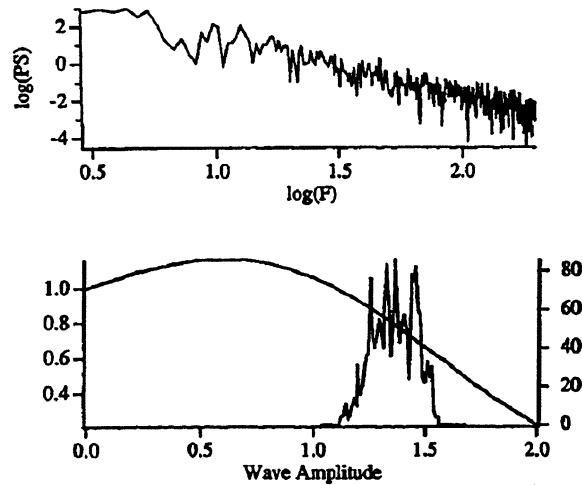


Fig. 10. The power spectrum and amplitude histogram are from the pulse density output of an element simulating a local neighborhood in the periglomerular population in the outer layer of the olfactory bulb (from [18]).

The third type of attractor gives aperiodic oscillation of the kind that is observed in recordings of EEGs. There is no one or small number of frequencies at which the system oscillates. The system behavior is therefore unpredictable, because performance can be projected well into the future only for periodic behavior. The existence of aperiodic oscillation, now widely known as ‘chaotic’, was known a century ago, but systematic study was possible only after the full development of digital computers. The best known systems with

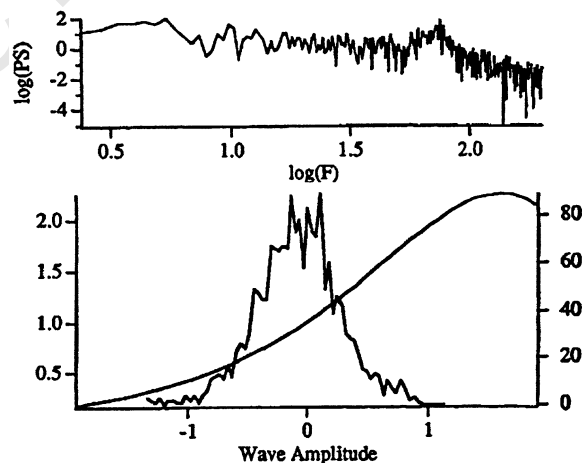


Fig. 11. The power spectrum and amplitude histogram are from the pulse density output of an element simulating a local neighborhood in the mitral cell population, the projection neurons of the olfactory bulb (from [18]).

chaotic attractors have a small number of components, finite fractal dimension, and few degrees of freedom, as for example, the double-hinged pendulum, the dripping faucet, and the Lorenz, Chua, and Rössler attractors. These simple models are stationary, autonomous, and noise-free, belonging to the class of ‘deterministic chaos’.

Large and complex real-world systems, which include neurons and neural populations are noisy, infinite-dimensional, non-stationary, non-autonomous, yet they are capable of rapid state transitions, indicating behavior that is distinguished as ‘stochastic chaos’ [15]. The source in the olfactory bulb has been shown to be the synaptic interaction of millions of mutually excitatory neurons, which create a 2-D field of microscopic brown noise in the bulb, but which are constrained by their relative and absolute refractory periods to generate a mesoscopic order parameter (a steady-state excitatory bias under brainstem control) that regulates the threshold for state transitions to form the spatiotemporal AM patterns of cortical activity revealed by the EEG. The bias provides the bifurcation parameter that takes the olfactory system from a point attractor under deep anesthesia (*figures 6, 7*) to a chaotic attractor in waking rest, and then to the level of arousal at which the volleys of action potentials from receptors in the nose during inhalation can readily change the landscape and induce a state transition to one of the newly actualized basins of attraction (*figure 8*, ‘inhalation’).

EEG recordings from epidural electrode arrays fixed permanently onto the visual, auditory, and somesthetic cortices have shown that each sensory cortex (comparable in this respect to the olfactory bulb, the first cortical stage in smell) maintains multiple basins corresponding to previously learned classes of stimuli, as well as to the unstimulated state, which together form an attractor landscape. The postulate here (*figure 2*) is that preafferent input [33, 34] from the limbic system can serve to bias the landscape in such a way as to facilitate the capture of the system by a basin of an attractor (*figure 8*) corresponding to the goal of the intended observation, perhaps in the manner of the variable tiling in a Voronoi diagram. Thereby basins of attraction in each of the sensory cortices are shaped by limbic input to sensitize the reception of the desired class of stimuli in every modality. These chaotic prestimulus states of expectancy establish the sensitivities of the cortices, so that the very small number of sensory action potentials evoked by expected stimuli can carry the

cortical trajectories into the basins of appropriate attractors in each modality, irrespective of which equivalent receptors actually receive the expected stimuli. In the absence of the stimulus, the cortices continue to transmit their output to the limbic system, confirming the continuing absence. The prefference is facilitated by the motor systems through orientation of the sensory receptors in space by sniffing, looking and listening.

#### 4. Understanding brain chaos by modeling with differential equations

The discovery of chaos has profound implications for the study of brain function [45]. A chaotic system has the capacity to create novel and unexpected patterns of activity. It can jump in a virtual instant from one mode of behavior to another, because it has a collection of attractors, each with its basin, and it can move from one to another in an itinerant trajectory [53]. It retains in its pathway across its basins its history, which fades into its past, just as its predictability into its future decreases. Transitions between chaotic states constitute the dynamics that we need model in order to understand how brains do what they do.

##### 4.1. The importance of noise for stabilization of brain chaos

Systems that model neurons and brains with networks of nonlinear ordinary differential equations (ODEs) have multiple point, limit cycle and chaotic attractors, each with its basin of attraction, which serves to provide the generalization gradient required for classification of recurring stimuli that are never twice the same. If the basin is that of a point or a limit cycle attractor, the system can proceed to a predictable and identical end state. If the basin leads to a chaotic attractor, the system goes into ceaseless fluctuation, as long as its energy lasts. If the starting point is identical on repeated trials, which can only be assured by simulation of the dynamics on a digital computer, the same aperiodic behavior appears. If the starting point is changed by an arbitrarily small amount, although the system is still in the same basin, the trajectory is not identical. A deterministic chaotic system that is in the basin of one of its chaotic attractors is legendary for its sensitivity to the initial conditions. If it is not known to an observer whether

there is a difference in starting conditions, the observer can infer the difference from the unfolding behavior of the system, if a difference in trajectories becomes apparent. This outcome shows that a chaotic system has the capacity to create information in the course of continually constructing its own trajectory into the future, but that the information exists not in the system but in the relation of the observer to the system. That information is not useful for pattern classification in the circumstance that every new stimulus of the same class is different in irrelevant detail from any preceding, so that while the deterministic chaotic system provides extreme sensitivity, it does not readily provide for generalization.

Stochastic chaotic systems feed on noise, which makes them robust in respect to initial conditions and therefore suitable for pattern recognition. Digital simulation of stochastic chaotic dynamics presents special problems, due to the discretization that is inherent in using rational numbers instead of real numbers to simulate continuous variables in time, space and intensity. Large systems using > 100 ODEs suffer from an explosion of attractors of all types, leading to the phenomenon of 'attractor crowding' [59], in which the size of the basins shrinks until it approximates the step size in digital simulation. Tracking the true 'shadowing trajectory' [22, 24] by discrete steps in numerical integration, like trying to walk a straight line such as a curbstone while intoxicated. When the true trajectory comes close to the edge of a chaotic basin with a fractal boundary, measured in terms of the number of bits in digital approximation of the continuum, the next discrete step takes the system into the adjacent basin, which is most likely to be that of a point or limit cycle attractor, and which will lock the system into a perseverative computational loop. With elapsed time this numerical failure becomes virtually certain. For example, in simulation of EEGs with the KIII model [14] incorporating  $\sim 920$  ODEs that are solved using double precision arithmetic giving a precision of 1 part in  $10^{16}$ , the model escapes from its designated chaotic basin in a simulated run time of  $\sim 1.5$  s, and it must then be shut down and restarted.

In the KIII model of the olfactory system this problem of numerical instability has been solved by the introduction of a random number generator (which is actually a deterministic chaotic generator that is capable of demonstrating the sensitivity to initial conditions) to simulate additive noise modeled on noise sources in the olfac-

tory system. Two types of noise are used at a level of 5–15% of the amplitude of the state variables: full wave rectified noise independently generated at each input to simulate the excitatory receptor pulse densities, and Gaussian noise to the element corresponding to the anterior olfactory nucleus to simulate the sum of centrifugal input to the olfactory system constituting spatially coherent noise [18]. The additive noises suffice to stabilize the digitally embodied attractors [32, 38], and they enhance the capabilities of the KIII model for pattern classification. This is analogous to the use of noise to improve system performance in stochastic resonance [5] and in simulated annealing [38], but those uses serve to destabilize systems that are captured by local minima, whereas the noise in the KIII model serves to expand the basins of the learned attractors, which otherwise are excessively narrow.

Examples are shown (*figure 9*) of simulated activity densities from the olfactory bulb (the periglomerular cells and the mitral cells), the anterior olfactory nucleus (pyramidal cells) and the prepyriform cortex (the superficial pyramidal cells), which generate the EEGs. The transient stage of initialization takes about 250 ms. An example is shown in *figure 10* of the power spectral density versus frequency in Hz in log-log coordinates for the periglomerular cell pulse density as a function of time (upper frame) after the steady state has been reached. The amplitude histogram is shown in the lower frame, superimposed on the relevant portion of the nonlinear gain curve (*figure 5*) at the appropriate value for the maximal asymptote,  $Q_m = 1.7$ . As explained in text, the location of the distribution of amplitudes of pulse density above the maximal gain, here at the natural logarithm of wave amplitude of 0.53, is predicted from the fact that the periglomerular cell population is governed by a non-zero point attractor (the zero point attractor being displayed under deep anesthesia (*figure 6*)). The example of the power spectral density (*figure 11*) reveals in the gamma range (20–80 Hz) the excess of power above a linear  $1/f^2$  relation that is characteristic of olfactory system EEGs. The amplitude densities are distributed about a mean wave amplitude near zero, and below the peak of the gain curve at wave amplitude of 1.6 (natural logarithm of the maximal asymptote,  $Q_m = 5.0$  (*figure 5*)). The location of this distribution is consistent with the governance of the mixed population of excitatory and inhibitory bulbar neurons by a limit cycle attractor. However, periodic oscillation in the bulbar

EEG is only seen when the bulb has been isolated from the rest of the olfactory system. The anterior nucleus and prepyriform cortex also have characteristic frequencies that are measured as in the bulb from averaged evoked potentials [14], but the three frequencies are incommensurate (not in integer ratios), so when they are coupled by feedback into a neural ‘ménage à trois’, and chaotic oscillation results.

#### 4.2. Measuring phase by fitting wavelets with nonlinear regression to EEGs

The aperiodic carrier wave form of each spatial AM pattern has a dominant or ‘center’ frequency of the oscillation, at which the phase can be determined with respect to the phase of the spatial ensemble average. Measurements of phase were made to test three predictions. The first was that phase gradients would be detected in spatial patterns of gamma bursts, which would correspond to the direction and velocity of the afferent pathways, as had already been demonstrated in the spatial patterns of oscillatory evoked potentials on electrical stimulation of the afferent axons to the olfactory bulb and to the prepyriform cortex [9]. The second prediction was that the phase distribution in olfactory AM patterns would be converged (narrowed) during a sniff of a familiar odorant, indicating an approach of the distribution of oscillations to ‘zero time lag’ [35, 41], which was based on the ‘binding’ hypothesis [25, 42]. The third prediction was that the width of the distributions of phase within AM patterns would be limited to a range in which those patterns could be extracted by spatial integration without degradation by excessive phase lag (which would occur beyond  $\pm 45^\circ$ , at which the shared power is half the total).

EEG traces were measured by decomposing them with appropriate basis functions. In the Fourier case, the basis functions were cosines giving the phase and amplitude of frequencies in the gamma range. Whereas accurate measurement of amplitude was relatively easy, measurement of the phase was subject to large errors owing to the brief duration of segments, the small number of cycles in each segment, the strong tendency to frequency modulation (FM) and amplitude modulation (AM) about center frequencies and amplitudes in both time and space, and the mix of multiple frequencies in spectra of most segments, especially from neocortices with their tendency to ‘ $1/f^2$ ’ spectra [2]. An alternative was to use wavelets, which

were cosines linearly modulated in amplitude (AM) and frequency (FM) in time about center values [21]. The sum of two wavelets was fitted to the 64 EEG traces in concomitantly recorded segments lasting 64–128 ms by nonlinear regression, using the least mean square residuals as the criterion of convergence, each wavelet being given by:

$$\begin{aligned} \text{EEG}(\tau) &= \sum_{n=1}^2 v_{n,i} [1 + \text{AM}_i](\tau - \tau_m) \\ &\quad \times \cos\{2\pi f_n[\text{FM}_i(\tau - \tau_m)]\tau + \varphi_{n,i}\} + \varepsilon(\tau), \\ &\quad i = 1, 64(2) \end{aligned} \quad (2)$$

where  $n = 1, 2$  was the number of the wavelet,  $v_{n,i}$  was mean amplitude of the  $i$ -th component,  $\text{AM}_i$  and  $\text{FM}_i$  were fixed coefficients to represent linear amplitude and frequency modulation across the center of the time segment,  $\tau_m$ ,  $f_n$  was the common center frequency of wavelet oscillation,  $\varphi_{n,i}$  was the desired phase of onset of the  $i$ -th damped cosine, and  $\varepsilon(\tau)$  was the residual noise after fitting the sum of two cosines to the EEG( $\tau$ ) segment. The sum was fitted in stages to the spatial ensemble average EEG in order to estimate the frequency, modulation coefficients, and the reference phase,  $\varphi_n$ , with respect to which all other 64 phase values,  $\varphi_{n,i}$ , and mean amplitudes,  $v_{n,i}(\tau)$ , were estimated by fitting the same sum of two component cosines to each of the 64 traces,  $i = 1, \dots, 64$ .

The standard error of measurement (SEM) was estimated by measuring a single cosine embedded in noise in 64 traces at zero phase and varying amplitudes corresponding to observed EEG amplitude distributions in AM patterns, with preset levels of random numbers filtered in the same way as the EEGs to give specified signal:noise ratios [16, 21]. The results gave a SEM that averaged about  $\pm 60^\circ$  for a single cosine fitted to raw EEGs. The SEM was reduced to  $\pm 6^\circ$  after application of appropriately designed wavelets spatial and temporal pre-filters, which have since been used in all studies requiring the phase measurements presented here.

A major problem in correlation of intentional behavior with neocortical EEGs (as compared with olfactory EEGs) was temporal segmentation. The location of spatial AM patterns in the gamma range of olfactory EEGs was simplified by the prominent respiratory wave in the theta range and the associated temporal AM revealing bursts of gamma oscillations. Contrariwise, visual inspection of the neocortical EEGs gave no indication of

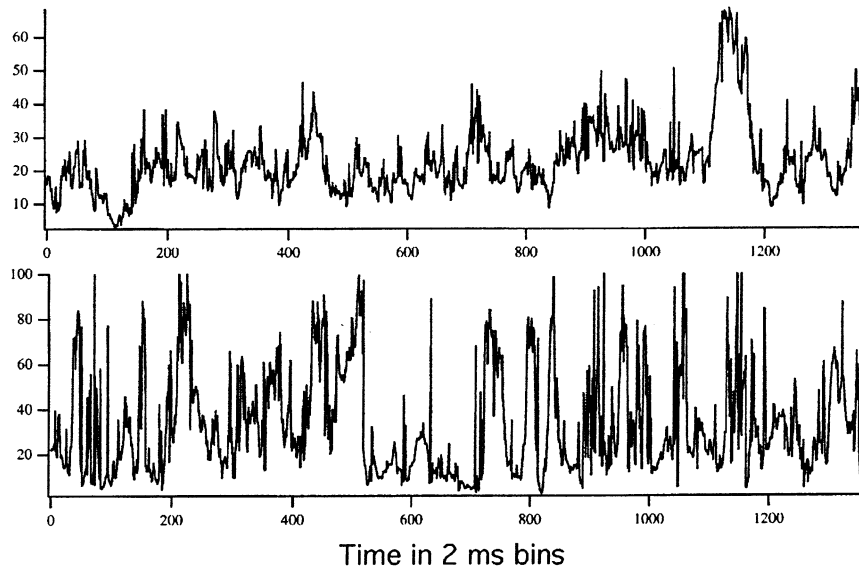


**Fig. 12.** Upper frame: % The time series of residuals is from repeatedly fitting equation (2) by nonlinear regression to EEG segments lasting 62 ms (32 time points at 2 ms intervals). Time is in 2-ms bins after stimulus arrival at 0. Lower Frame: % Residuals from nonlinear regression of a cone onto the 64 values of phase from the dominant wavelet ( $n = 1$  in equation (2)) fitted to the 64 EEG traces at each frame step. The reference phase was that of the spatial ensemble average. Acceptable fit for cone detection was  $< 20\%$  residuals.

where AM pattern segments might start or end, either by any distinctive wave in the theta and alpha ranges, or by any temporal AM in the gamma range. Therefore, a fixed-duration segment was stepped along the multiple EEG traces on every trial. The measurement procedure was repeated on 32-bin (64 ms) segments stepped at 2 bin (4 ms) overlapping intervals over time. The goodness of fit of the two cosines to the 64 EEG traces was shown by plots of residuals. An example of the results from a single trial is shown in *figure 12*, upper frame, where residuals  $< 20\%$  was adopted as a criterion of successful fit.

#### 4.3. Testing predictions of properties of spatial phase distributions

The first prediction, that gamma phase gradients would correspond in direction and slope to the direction and conduction velocity of afferent axons, was confirmed for the prepyriform cortex but not for the olfactory bulb, despite the fact that the spatial phase gradients of the bulbar oscillations evoked by single-shock electrical stimulation of the primary olfactory nerve conformed to the properties of its axons [9]. About 50% of the variance of the 64 phase values was captured by a plane, but the orientation of tilt of the plane varied randomly from each AM pattern to the next, and without

relation to the conditioned stimuli used for testing behavioral discrimination. The second prediction, that the phase distribution would narrow or collapse on arrival of an expected conditioned stimulus and formation of an AM pattern signaling 'binding', failed in both the bulb and the prepyriform cortex. No differences in the standard deviations of phase distributions were found between control and test periods. The third prediction, that the distributions of phase values would be less than  $\pm 45^\circ$ , was confirmed within the window of the arrays ( $4 \times 4$  to  $6 \times 6$  mm), but the entire surfaces of the structures being recorded from were inaccessible for direct observation.

Visual inspection of 2-D contour plots of bulbar numerical phase values not uncommonly revealed radial symmetry in the form of concentric isophase contours. With this clue the phase distributions of AM patterns were fitted using nonlinear regression with a cone having the parameters of location in 2-D of the apex and the slope of the cone, including its sign. The goodness of fit improved substantially over fitting a plane to the phase data. The results from three sessions of twenty trials in each of five rabbits are shown in *figure 13*, in which the size and location of the array was superimposed on an outline of the olfactory bulb, the bulb was approximated by a sphere, and the bulbar surface was displayed as a flattened sphere [16]. The apices

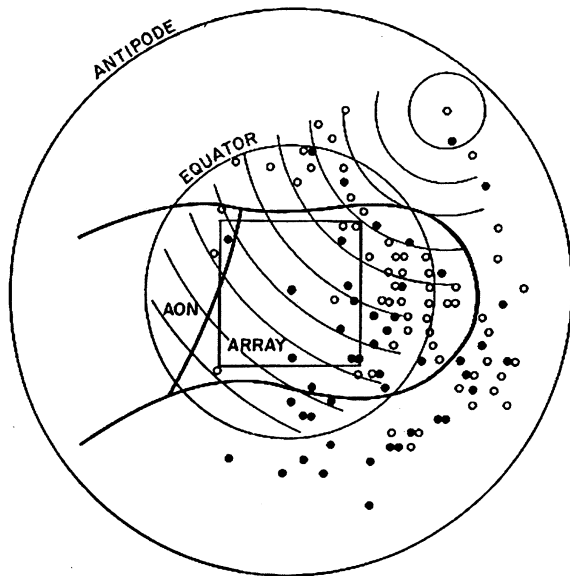


**Fig. 13.** Phase distributions were measured with respect to the phase of the spatial ensemble average at the surface of the olfactory bulb and fitted with a cone in spherical coordinates. The sketch is a projection of the outline of the bulb as it would appear on looking through the left bulb onto the array on the lateral surface of the bulb. A representative set of isophase contours is at intervals of  $0.25 \text{ radians} \cdot \text{mm}^{-1}$ . The locations of the apices of the cones on the surface of the sphere (2.5 mm in radius) are plotted from the center of the array to the antipode. The square outlines the electrode array. The standard error of location of points was twice the radius of the dots (from [16]).

were extrapolated to locations anywhere on the surface, but not to the posterior quadrant where the connections to the forebrain are located, and without relation to the stimulus conditions or to

the amplitude peaks or valleys in the accompanying AM patterns. The signs of the apices (lead indicated by a solid dot and lag by an open dot) varied at random on sequential trials. The slopes of the phase cones measured in radians/mm varied with gamma frequency in Hz, but when converted to  $\text{m} \cdot \text{s}^{-1}$  using the frequency converged to an invariant at  $1.82 \text{ m} \cdot \text{s}^{-1}$ , which was the estimated frequency of axon collaterals of mitral and tufted cells running in the bulb parallel to the surface. Considering the distance around the bulb at the level of the internal plexiform layer, the estimated maximal phase difference between any two points in the mitral cell layer was estimated to be less than  $\pm 45^\circ$  over the full gamma range (20–80 Hz).

Comparable spatial phase cones have been found in conjunction with AM patterns in visual, auditory, and somesthetic EEGs, both by Fourier decomposition [17] and by use of wavelets (equation (2)) and nonlinear regression. A typical sequence of goodness of fit in terms of % residuals from the post-stimulus segment of a single trial is seen in *figure 12*, lower frame, where  $< 20\%$  residuals was adopted as one of several criteria for determining the presence of a cone. A raster plot in *figure 14* shows an example of the time locations of recurring phase cones in a set of forty trials. *Figure 15* shows the spectrum of the autocovariance of the cones in the forty trials laid consecutively in comparison with the autospectrum of autocovariance of the concomitant spatial ensemble average of the EEG and the cospectrum. In every rabbit and session a prominent peak was found in the theta range (2–7 Hz) of the cospectrum of the phase cones and the EEG. A peak in power was found often but not always at the same

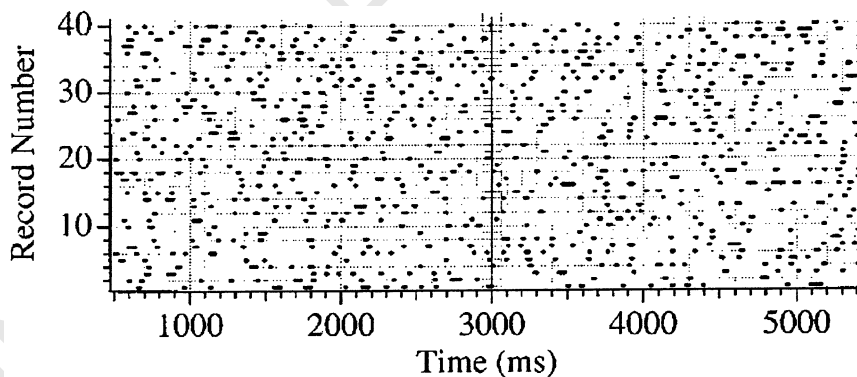


**Fig. 14.** Distribution are shown by line segments of the times of occurrence of phase cones during forty trials by one rabbit in one session. Data are from visual cortex; the cones were fitted in planar coordinates. Each trial lasted 6 s (the display is truncated at 400 ms and 5600 ms by temporal filtering), with the stimulus arriving at the middle (3000 ms). The phase cones occur equally often in the control and test periods, as expected in self-organizing cortical dynamics.

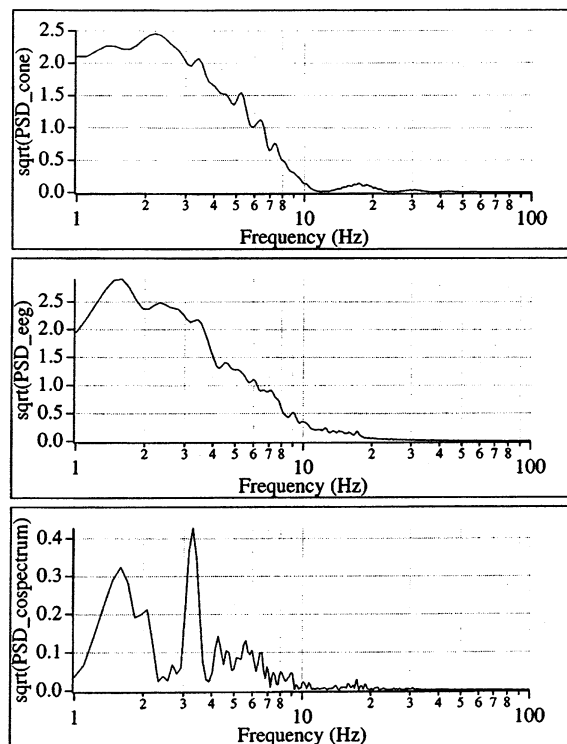


**Fig. 15.** The spectrum of the autocovariance of the cones in the forty trials laid consecutively is compared with the autospectrum of the autocovariance of the concomitant spatial ensemble average of the EEG and the cospectrum. The peak in the theta range of the cospectrum is an indication that a destabilizing 'forcing function' originating extracortically operates on the sensory neocortices in a manner similar to the role of respiration in olfaction [14].

frequency in the EEG autospectrum, but a peak was seen rarely in the autospectrum of the phase cones.

As in the olfactory bulb the locations and signs of the apices of the phase cones varied at random over successive events, and the frequencies of the gamma oscillations varied also. Typical distributions are shown in *figure 16* of the center frequencies in Hz and the slopes in  $\text{radians} \cdot \text{mm}^{-1}$ . From these were calculated the phase velocities in  $\text{m} \cdot \text{s}^{-1}$  (which are consistent with reports of the distributions of conduction velocities of neocortical axons [47, 17]), and the radii to the phase contour at  $\pm 45^\circ$ , from which the half-power diameters indicated by the phase cones were calculated.

#### 4.4. Radial phase gradients provide physiological evidence for first order cortical state transitions

Several inferences follow from these findings. First, the common wave form found in traces from

the 64 electrodes cannot be ascribed either to activity at the reference electrode on monopolar recording or to volume conduction from a single current generator under the array, because of the systematic differences in phase. Nor is it due to decorrelation with distance over a distribution of noise generators smeared by volume conduction [6], because that would not give radial phase gradients. Nor does it allow for progressive entrainment of coupled oscillators, because the phase gradients persist through the segments, indicating that a phase gradient established in the time of transition lasting a few ms persists through the 80–120 ms duration of the AM pattern, probably owing to the sparseness of the local connection densities [4, 17], which fail to support convergence of activity into zero time lag synchrony within the duration of the patterns. These results, however, give support to recent findings of the spatial coherence of gamma activity recorded on the scalp of humans performing cognitive tasks [48, 49], because the size of the AM patterns in cm may allow detection of the gamma bursts in scalp EEGs.

Second, the random variation of the sign of the apices cannot be explained by an intracortical or thalamic pacemaker, which could only have phase lead whether acting by excitation or inhibition. It is compatible with a symmetry-breaking state transition such as a saddle node bifurcation. The property of mesoscopic states that makes them interesting is the capacity they give to large populations of neurons for rapid changes in the global spatiotemporal patterns of organization and function. Some well known examples are the transitions between waking and sleeping states, between vocalizing and swallowing, and between walking and running, by which the neurons widely distributed in the brain and spinal cord shift their firing from one coordinated pattern to the next globally in a few ms. Evidence from physical distributed systems shows that state transitions do not start simultaneously throughout the systems but begin at a 'site of nucleation' and spread radially, as in the formation of a snowflake or raindrop around a dust particle. The radial phase patterns in the EEG provide strong evidence that AM patterns form by self-organizing cortical state transitions. They indicate that the cortical activity manifested in the EEGs is not shaped directly by sensory or other external sources of pulses, but instead that it is endogenously constructed following state transitions that direct the cortices through attractor landscapes yielding differing spatial patterns [11–16]. In the olfactory system it

is apparent that the state transitions depend on receptor input, which provides a behaviorally related ‘forcing function’ that can destabilize the bulb. If this hypothesis is correct, then the formation of AM patterns and phase cones in neocortex requires comparable forcing functions. Evidence for these is not readily seen in EEGs, but seems unequivocal in cospectra of EEGs with sequences of phase cones. Further evidence for forcing functions should be sought in behaviors such as saccades in vision, finger tremor in touch, and

effluent control of muscles in the middle ear in audition.

Third, the delays in axonal propagation manifested in the phase cones may serve to delimit soft spatial boundaries of neocortical AM patterns during both construction and read-out. The neocortical neuropil forms a continuous sheet, as shown by the phenomenon of spreading depression of  $\text{Lea}\delta$  [3], which stops only at the borders of the neocortex in each hemisphere with the archicortex and the callosum. The submillimeter mi-

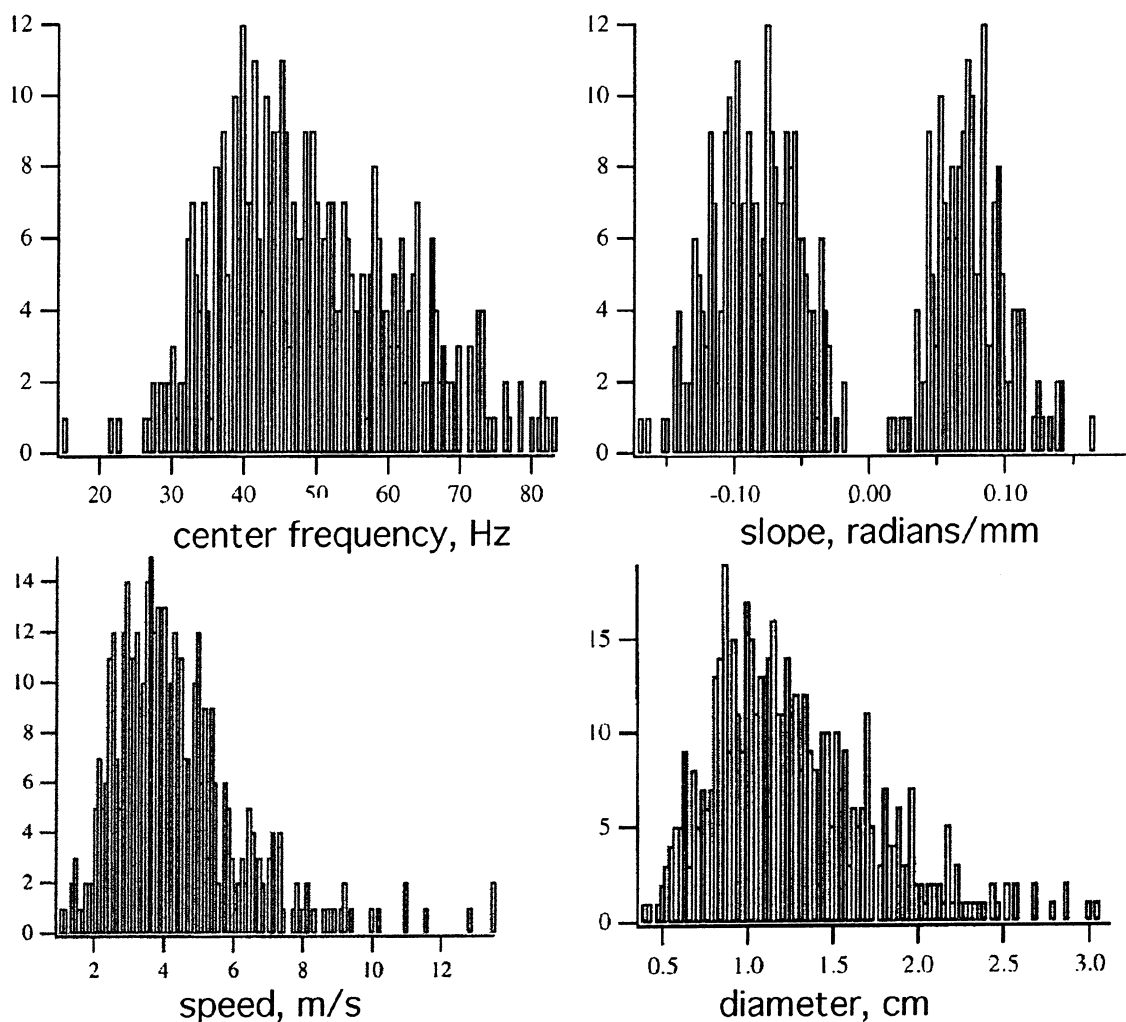


**Fig. 16.** Upper left: An example is shown of the distribution of center frequencies (Hz) of phase cones. Upper right: The distribution of slopes ( $\text{radians} \cdot \text{mm}^{-1}$ ) of phase cones, was bimodal, showing equal probability of maximal lead or lag at apices. Lower left: The phase velocities of slopes calculated from the center frequencies were compatible with estimates of the conduction velocities of axons running parallel to the pia, which are slower than so-called ‘U-fibers’ running deeply from one area of cortex to another. Lower right: The mode of the distribution of half-power diameters is about 1.1 cm, which is much larger than the sizes of cortical columns and hypercolumns.

croscopic architecture of cortex is spatially coarse-grained by its input projections into cortical columns and barrels, which are smaller by an order of magnitude than the mesoscopic AM patterns. The EEGs of cortical areas that are separated by macroscopic distances lack high spatial coherence, giving evidence that the mesoscopic AM patterns must have soft boundaries. The obligatory axonal propagation delays may provide the neocortical dynamic boundary conditions, which are required to give the different areas a requisite degree of autonomy, while not freezing them into anatomically fixed arrangements. Within each area, the spatially coherent EEGs manifest cooperative interactions among millions of neurons, but cooperativity must weaken with phase dispersion. The radial phase gradients can serve to attenuate mesoscopic synaptic interactions with distance. With no hard edges the half-power radius ( $\pm \cos 45^\circ$ ) can serve to define the sizes and locate the soft boundaries for local cooperative domains, at the interface between microscopic neural activity and cortical mesoscopic states. The cosine values then provide a measure of the degree of relatedness of the gamma activity within a temporal segment of the EEG in a mesoscopic cortical area.

Fourth, the classification of AM patterns with respect to CSs reveals that the classificatory information is homogeneously distributed in space; no channel is any more or less important than any other [2, 16, 20]. This property shows that the information relating to the topographic mapping of the sensory input has been spatially disseminated by the dynamic operation of constructing AM patterns. The independence of the mesoscopic pattern from the details of the input-dependent cortical architecture may be critical for the integration of multisensory percepts, in which the local space-time gradients peculiar to the retinal, cochlear and cutaneous mappings are no longer relevant.

Fifth, phase cones are not detected in prepyriform cortex, which leads to the suggestions that they are a property of self-organizing dynamics in primary sensory areas of cortex, and that a secondary area of cortex is required to be driven by the AM pattern in order to transform it to a new pattern that is compatible with input requirements of other parts of the brain. In other words, pairs of cortices may work in tandem, one to produce the AM patterns, the other to prepare it for further transmission, and to serve as the chaotic controller of the first cortex. If so, then the phase cone serves as an identifying property of the first type in

sensory neocortex, and a search should be made for cortices of the second type corresponding to the role of the prepyriform cortex as a controller in the genesis of chaotic activity.

## 5. Conclusions

The sensory cortices are conceived as being bistable, having serial receiving and transmitting modes that subservise 'feature binding' during diastole and the formation and transmission of perceptual constructs in AM 'wave packets' [9] during systole forced by input. Each burst constitutes the systolic output of a sensory area, which is prepared during a pre-burst diastolic period of sensory intake ending in a first order state transition, and which is constructed by the self-organizing attractor dynamics of the neural population in each area. Whatever the clean logical functions of cortical microscopic neural networks might be, the nonlinear dynamics of cortices at the mesoscopic level by this hypothesis are neither autonomous, stationary, or noise-free, but engaged with input and output, undergoing repeated changes in state, and embedded in the noise of myriads of microscopic action potentials constituting mesoscopic biases [13, 14].

These considerations lead to the inference that the wave packets are formed by cooperative synaptic interactions within areas of cortex on a mesoscopic scale greater than the microscopic time and space scales of the component neurons, but smaller than the macroscopic scales of domains shown by brain imaging based on metabolic and hemodynamic processes. These mesoscopic interactions shape the spatial AM patterns owing to changes in intracortical synaptic strengths from cumulative effects of reinforcement learning. Each successive spatial AM pattern is formed by a nonlinear state transition having an estimated state transition time on the order of 6 ms and a modal diameter on the order of 5 to 10 mm, considerably greater than the dimensions of the dendritic arbors of most neurons and the estimated sizes of cortical columns and hypercolumns, but less than the dimensions of the lobes of the forebrain and, in small mammals, the cerebral hemispheres [17].

The significance of these findings and inferences lies in the possibility that the spatial coherences manifest mesoscopic integrative processes by which information that is injected into cortical activity sensory receptors through thalamic relays is integrated into perceptual forms shaped by life-

long prior learning. If so, the processes offer an alternative to a widely entertained form of the ‘binding’ hypothesis [44, 56], which holds that the pulse trains of a small network of microscopic neurons are locked in zero phase and zero time lag synchrony [52, 54]. Instead, the binding revealed at the mesoscopic level consists in a small covariant fraction of the total variance of all the neurons within the diameter of a wave packet imposed by cooperative dynamics, which provides fixed phase values of the oscillating probabilities of neural firing over its time duration, but which imposes a distribution of their phase values over its spatial extent.

These new data and inferences have profound implications for studies of cognitive brain functions in humans, because they open the way to experimental investigations of human EEG activity both at the scalp and at the pial surface by giving assurance that recording with high-density electrode arrays can yield information of great value for understanding normal cognition and diagnosing and treating cognitive disabilities [20], arising primarily from disorders at the mesoscopic level and secondarily manifesting themselves at the microscopic level in biochemical abnormalities and at the macroscopic level in distressed behaviors. These findings also are important for engineers in the design of new kinds of intelligent machines [14], in which the emphasis is placed on self-organization and the emergence of intentional behavior that is created by nonlinear dynamics modeled on the distributed, continuous-time dynamics of the cerebral cortex at the mesoscopic level.

### Acknowledgements

This work was supported by grants from the National Institute of Mental Health MH06686, the Office of Naval Research N00014-90-J-4054, and from ARO MURI DAAH04-96-1-0341.

### References

- [1] Aquinas St. Thomas, *Treatise on Man*, Chapters in: *Summa Theologica*, translated by Fathers of the English Dominican Province, revised by Sullivan D.J., vol. 19, Great Books Series, Encyclopedia Britannica, Chicago IL, 1952/1272, pp. 378–487.
- [2] Barrie J.M., Freeman W.J., Lenhart M., Modulation by discriminative training of spatial patterns of gamma EEG amplitude and phase in neocortex of rabbits, *J. Neurophysiol.* 76 (1996) 520–539.
- [3] Bures J., Buresová O., Krivánek J., *The Mechanism and Applications of Leão’s Spreading Depression of Electroencephalographic Activity*, Academic Press, New York, 1974.
- [4] Braitenberg V., Schüz A., *Anatomy of the Cortex: Statistics and Geometry*, Springer-Verlag, Berlin, 1991.
- [5] Carroll T.L., Pecora L.M., Stochastic resonance and chaos, *Phys. Rev. Lett.* 70 (1993) 576–579.
- [6] Elul R., The genesis of the EEG, *Int. Rev. Neurobiol.* 15 (1972) 227–272.
- [7] Emery J.D., Freeman W.J., Pattern analysis of cortical evoked potential parameters during attention changes, *Physiol. Behav.* 4 (1969) 67–77.
- [8] Freeman W.J., Patterns of variation in wave form of averaged evoked potentials from prepyriform cortex of cats, *J. Neurophysiol.* 31 (1968) 1–13.
- [9] Freeman W.J., *Mass Action in the Nervous System*, Academic Press, New York, 1975.
- [10] Freeman W.J., A physiological hypothesis on perception, *Perspect. Biol. Med.* 24 (1981) 561–592.
- [11] Freeman W.J., Tutorial in neurobiology: From single neurons to brain chaos, *Int. J. Bifurcation Chaos* 2 (1992) 451–482.
- [12] Freeman W.J., *Societies of Brains*, Lawrence Erlbaum Associates, Mahwah NJ, 1995.
- [13] Freeman W.J., Noise-induced first-order phase transitions in chaotic brain activity, *Int. J. Bifurcation Chaos* 9 (1999) 2215–2218.
- [14] Freeman W.J., *Neurodynamics. An Exploration of Mesoscopic Brain Dynamics*, Springer-Verlag, London, 2000.
- [15] Freeman W.J., A proposed name for aperiodic brain activity: Stochastic chaos, *Neural Networks* 13 (2000) 11–13.
- [16] Freeman W.J., Baird B., Relation of olfactory EEG to behavior: spatial analysis, *Behav. Neurosci.* 101 (1987) 393–408.
- [17] Freeman W.J., Barrie J.M., Analysis of spatial patterns of phase in neocortical gamma EEGs in rabbit, *J. Neurophysiol.* 84 (2000) 1266–1278.
- [18] Freeman W.J., Chang H.J., Burke B.C., Rose P.A., Badler J., Taming chaos: stabilization of aperiodic attractors by noise, *IEEE Trans. Circuits Syst.* 44 (1997) 989–996.
- [19] Freeman W.J., Grajski K.A., Relation of olfactory EEG to behavior: Factor analysis, *Behav. Neurosci.* 101 (1987) 766–777.
- [20] Freeman W.J., Rogers L.J., Holmes M.D., Silbergeld D.L., Spatial spectral analysis of human electrocorticograms including the alpha and gamma bands, *J. Neurosci. Meth.* 95 (2000) 111–121.
- [21] Freeman W.J., Viana Di Prisco G., Relation of olfactory EEG to behavior: time series analysis, *Behav. Neurosci.* 100 (1986) 753–763.
- [22] Fryska S.T., Zohdy M.A., Computer dynamics and shadowing of chaotic orbits, *Phys. Lett. A* 166 (1992) 340–346.
- [23] Goltz F.L., *Der Hund ohne Grosshirn. Siebente Abhandlung über die Verrichtungen des Grosshirns*, *Pflügers Arch.* 51 (1892) 570–614.

- [24] Grebogyi C., Hammel S.M., Yorke J.A., Sauer T., Shadowing of physical trajectories in chaotic dynamics: containment and refinement, *Phys. Rev. Lett.* 65 (1990) 1527–1530.
- [25] Gray C.M., Synchronous oscillations in neuronal systems: mechanisms and functions, *J. Comp. Neurosci.* 1 (1994) 11–38.
- [26] Haken H., *Synergetics: An Introduction*, Springer-Verlag, Berlin, 1983.
- [27] Hardcastle V.G., Psychology's binding problem and possible neurobiological solutions, *J. Consciousness Stud.* 1 (1994) 66–90.
- [28] Helmholtz H.L.F. von, *Handbuch der physiologischen Optik*, vol. 3, L. Voss, Leipzig, 1872/1909.
- [29] Herrick C.J., *The Brain of the Tiger Salamander*, University of Chicago Press, Chicago IL, 1948.
- [30] Jackson J.H., in: Taylor J., Walshe F.M.R., Holmes G. (Eds.), *Selected writings of John Hughlings Jackson*, Hodder and Stoughton, London, 1931.
- [31] James W., *The Principles of Psychology*, H. Holt, New York, 1893.
- [32] Kapitaneck T., *Chaos in Systems with Noise*, World Scientific, Singapore, 1988.
- [33] Kay L.M., Freeman W.J., Bidirectional processing in the olfactory-limbic axis during olfactory behavior, *Behav. Neurosci.* 112 (1998) 541–553.
- [34] Kay L.M., Lancaster L., Freeman W.J., Reafference and attractors in the olfactory system during odor recognition, *Int. J. Neural Syst.* 7 (1996) 489–496.
- [35] König P., Schillen T.B., Stimulus-dependent assembly formation of oscillatory responses: I. Synchronization, *Neural Comput.* 3 (1991) 155–166.
- [36] Kornhuber H.H., Deecke L. ((Eds.), *Motivation, Motor and Sensory Processes of the Brain: Electrical Potentials, Behaviour, and Clinical Use*, Elsevier/North-Holland, Amsterdam, 1990.
- [37] Libet B., *Neurophysiology of Consciousness: Selected Papers and New Essays*, Birkhauser, Boston, MA, 1994.
- [38] Liljenström H., Wu X.B., Noise-enhanced performance in a cortical associative memory model, *Int. J. Neural Syst.* 6 (1995) 19–29.
- [39] Merleau-Ponty M., *The Structure of Behavior*, translated by Fischer A.L., Beacon Press, Boston MA, 1942/1963.
- [40] O'Keefe J., Nadel L., *The Hippocampus as a Cognitive Map*, Clarendon, Oxford, UK, 1978.
- [41] Roelfsema P.R., Engel A.K., König P., Singer W., Visuo-motor integration is associated with zero time-lag synchronization among cortical areas, *Nature* 385 (1997) 157–161.
- [42] Roth G., *Visual Behavior in Salamanders*, Springer-Verlag, Berlin, 1987.
- [43] Sherrington C.S., *The Integrative Activity of the Nervous System*, Yale University Press, New Haven CT, 1906.
- [44] Singer W., Gray C.M., Visual feature integration and the temporal correlation hypothesis, *Annu. Rev. Neurosci.* 18 (1995) 555–586.
- [45] Skarda C.A., Freeman W.J., How brains make chaos in order to make sense of the world, *Behav. Brain Sci.* 10 (1987) 161–195.
- [46] Sperry R.W., Neural basis of the spontaneous optokinetic response, *J. Compar. Physiol.* 43 (1950) 482–489.
- [47] Swadlow H.A., Weyand T.G., Efferent systems of the rabbit visual cortex: laminar distribution of the cells of origin, axonal conduction velocities, and identification of axonal branches, *J. Compar. Neurol.* 203 (1981) 799–822.
- [48] Tallon-Baudry C., Bertrand O., Delpuech C., Pernier J., Stimulus-specificity of phase-locked and non phase-locked 40-Hz visual responses in human, *J. Neurosci.* 16 (1996) 4240–4249.
- [49] Tallon-Baudry C., Bertrand O., Peronnet F., Pernier J., Induced gamma-band activity during the delay of a visual short-term memory task in humans, *J. Neurosci.* 18 (1998) 4244–4254.
- [50] Titchener E.B., *An Outline of Psychology*, Macmillan, New York, 1907.
- [51] Tolman E.C., Cognitive maps in rats and men, *Psychol. Rev.* 55 (1948) 189–208.
- [52] Traub R.D., Whittington M.A., Stanford I.M., Jefferys J.G.R., A mechanism for generation of long-range synchronous fast oscillations in the cortex, *Nature* 383 (1996) 421–424.
- [53] Tsuda I., A new type of self-organization associated with chaotic dynamics in neural networks, *Int. J. Neural Syst.* 7 (1996) 451–459.
- [54] Usher M., Schuster H.G., Niebur E., Dynamics of populations of integrate-and-fire neurons, partial synchronization and memory, *Neural Comput.* 5 (1993) 570–586.
- [55] Viana Di Prisco G., Freeman W.J., Odor-related bulbar EEG spatial pattern analysis during appetitive conditioning in rabbits, *Behav. Neurosci.* 99 (1985) 962–978.
- [56] von der Malsburg C., How are nervous structures organized?, in: Basar E., Flohr H., Haken H., Mandell A.J. (Eds.), *Synergetics of the Brain*, Springer-Verlag, Berlin, 1983, pp. 238–249.
- [57] von Holst E., Mittelstaedt H., Das Refferenzprinzip, *Naturwissenschaften* 37 (1950) 464–476.
- [58] Walter W.G., *The Living Brain*, Norton, New York, 1963.
- [59] Wiesenfeld K., Hadley P., Attractor crowding in oscillator arrays, *Phys. Rev. Lett.* 62 (1989) 1335–1338.